

Significance of the refraction effect on the p - d elementary process in the (p, pd) reaction

Kazuki Yoshida,^{1,*} Yoshiki Chazono,² and Kazuyuki Ogata^{3,4}

¹*Advanced Science Research Center, Japan Atomic Energy Agency, Tokai, Ibaraki 319-1195, Japan*

²*RIKEN Nishina Center for Accelerator-Based Science, 2-1 Hirosawa, Wako 351-0198, Japan*

³*Department of Physics, Kyushu University, Fukuoka 819-0395, Japan*

⁴*Research Center for Nuclear Physics, Ibaraki, Osaka 567-0047, Japan*

(Dated: June 10, 2024)

Background: The proton-induced deuteron knockout reaction, (p, pd) , is one of the interests in the studies for probing the deuteron-like p - n correlation in nuclei. According to a recent study of the inclusive deuteron-induced reaction, $(d, d'x)$, the refraction effect of the deuteron has a significant effect on the elementary process, nucleon-deuteron (N - d) binary scattering inside a nucleus, of the reaction. In the paper, it is shown that proper treatment of the local N - d relative momentum in the elementary process is crucial in $(d, d'x)$ reactions at 100 MeV and below.

Purpose: In the present work, we investigate the deuteron refraction effect in the exclusive (p, pd) reactions. We also discuss the incident energy dependence of the refraction effect.

Method: The refraction effect on the p - d elementary process is taken into account by the local semiclassical approximation to the distorted waves. The results are compared with those obtained with the asymptotic momentum approximation, which is standardly applied to the distorted wave impulse approximation framework.

Result: It is shown that the refraction effect drastically changes the energy sharing distribution of the $^{16}\text{O}(p, pd)^{14}\text{N}$ reaction at 101.3 MeV and gives a better agreement with experimental data. In contrast, it is confirmed that the effect is negligibly small at 250 MeV.

Conclusion: We have clarified that the deuteron refraction effect is significant in the $^{16}\text{O}(p, pd)^{14}\text{N}$ reaction at 101.3 MeV and the experimental data are well reproduced. The refraction effect plays a significant role in both the shape and magnitude of the (p, pd) cross section, while the effect is negligible at 250 MeV.

I. INTRODUCTION

The quasi-free knockout reactions have been used for more than half a century to probe both the single-particle (s.p.) nature of a nucleon [1–9] and the α cluster states [10–34] of nuclei. These reactions have been described by the distorted wave impulse approximation (DWIA) framework [3, 4] and the experimental data have been well understood within this framework.

Recently, more exotic clusters, e.g., d , t , and ^3He , have become of interest [35, 36]. These clusters as well as the traditional α cluster will be intensively studied by the ONOKORO project [37] using cluster knockout reactions mainly at HIMAC, RCNP, and RIKEN RIBF in Japan.

The proton-induced deuteron knockout reaction, (p, pd) , is expected to be a probe for the p - n spatial and spin-isospin correlations, or, existence of deuteron, inside a nucleus. One of the difficulties in describing the (p, pd) reaction is the fragileness of the deuteron, which is not explicitly included in the standard DWIA. In order to incorporate this nature of the deuteron into a reaction theory, the continuum-discretized coupled-channels (CDCC) wave function [38–40] has recently been implemented into the DWIA framework, and the breakup and the reformation process of the p - n pair in the (p, pd) reaction is studied within a new framework called CDC-CIA [41]. Another difficulty is that the refraction of the

deuteron by the nuclear potential is larger compared to that of the nucleon. According to the recent study on inclusive $(d, d'x)$ reactions [42] using the semiclassical distorted wave model [43, 44], the refraction effect on the p - d elementary process has a significant impact. The same effect is expected in the exclusive (p, pd) reactions and it has to be also considered in combination with the CDCCIA framework.

It should be noted that, in Ref. [25], the refraction effect in the $^{120}\text{Sn}(p, p\alpha)^{116}\text{Cd}$ was investigated and found to be small. The main reason of this result is the strong absorption of α in the region where the refraction is important. In other words, both the real and imaginary potential for α are strong. Thus, the significant effect of the deuteron refraction found in Ref. [42] will suggest that the refraction of the deuteron is much more important than its absorption.

In the present work, we focus on the deuteron refraction effect on the p - d elementary process in the (p, pd) reaction within the DWIA framework and discuss to what extent the (p, pd) cross section is affected. There is a limited number of (p, pd) reaction experiments [45–50]. In Ref. [51], the data of $^{16}\text{O}(p, pd)^{14}\text{N}^*_{3.95\text{ MeV}}$ at 101.3 MeV [47] are reanalyzed using the finite-range DWIA (FR-DWIA) formalism with two types of p - d interactions (“all attractive” and “repulsive core”).

This paper is organized as follows. In Sec. II we recapitulate the DWIA framework with the local semiclassical momentum approximation (LSCA) [43, 44] and the asymptotic momentum approximation (AMA) [25]. We discuss that the finite-range nature of the p - d effective

* yoshida.kazuki@jaea.go.jp

interaction is partially taken into account in the position dependence of its matrix element in DWIA with LSCA. In Sec. III the inputs for the DWIA calculations are explained and the effect of the local momentum on the (p, pd) cross section is discussed based on DWIA calculations with LSCA and AMA. The relation between the present result and the FR-DWIA calculation [51] is also discussed in Sec. III B. Finally a summary is given in Sec. IV.

II. THEORETICAL FRAMEWORK

In the present work, we basically follow the DWIA framework [3, 4, 7, 52] to describe the (p, pd) reaction. Practical calculations are performed using a newly published code PIKOE [52]. The incoming proton, the outgoing proton, and the outgoing deuteron are denoted as particles 0, 1, and 2, respectively, and the target (residual) nucleus is by A (B). The total energy and the wave number vector are represented by E_i and \mathbf{K}_i ($i = 0, 1, 2, A$, and B), respectively. All the quantities with the superscript L are evaluated in the laboratory (target-rest) frame of the (p, pd) reaction, while those without the superscript are evaluated in the center-of-mass frame. As a characteristic ingredient in the present study, we use the local semiclassical approximation (LSCA) [43, 44] to describe the propagation of the distorted waves under nuclear potentials, which is nothing but the refraction of the reaction particle. This method, DWIA with LSCA, has already been applied to $(p, p\alpha)$ analyses in Ref. [25].

Neglecting the spin degrees of freedom in the scattering waves and the elementary process, the DWIA T -matrix of the (p, pd) reaction is given by [3, 7, 52, 53]

$$T = \int d\mathbf{R} ds \chi_1^{*(-)}(\mathbf{R}_1) \chi_2^{*(-)}(\mathbf{R}_2) t_{pd}(s) \chi_0^{(+)}(\mathbf{R}_0) \varphi_d(\mathbf{R}_2). \quad (1)$$

The deuteron cluster is assumed to be bound in s -wave, as we discuss such experimental data [47] in this study. The coordinates are defined as shown in Fig. 1, and $\chi_i(\mathbf{R}_i)$ is the distorted wave describing the scattering state of particle i with respect to the coordinate \mathbf{R}_i . The

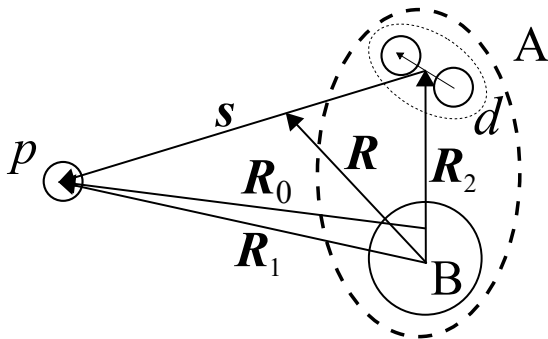


FIG. 1. Definition of the coordinates of the $A(p, pd)B$ reaction.

distorted waves with the superscripts (+) and (−) satisfy the outgoing and incoming boundary conditions, respectively. φ_d is a normalized bound state wave function of the deuteron and B, and its spectroscopic factor S_d is explicitly considered in Eqs. (13) and (16) below. t_{pd} is the p - d effective interaction which describes the p - d elastic scattering. In this study, it is assumed that t_{pd} does not change the p - n relative state and the p - n pair remains in the deuteron ground state and its breakup and reformation are not considered.

LSCA [43, 44] assumes that the short-range propagation from a reference point \mathbf{R} to $\mathbf{R} + \Delta\mathbf{R}$ is described by a plane wave with a local momentum $\mathbf{K}(\mathbf{R})$ at the reference point \mathbf{R} :

$$\chi_i(\mathbf{R} + \Delta\mathbf{R}) \approx \chi_i(\mathbf{R}) e^{i\mathbf{K}_i(\mathbf{R}) \cdot \Delta\mathbf{R}}. \quad (2)$$

This is the first order approximation of a translation by $\Delta\mathbf{R}$ of $\chi_i(\mathbf{R})$. The norm of $\mathbf{K}_i(\mathbf{R})$ is determined by local energy conservation and the direction of $\mathbf{K}_i(\mathbf{R})$ is taken to be parallel with the flux of $\chi_i(\mathbf{R})$. LSCA has been applied to the scattering of nucleon [43, 44, 54], α particle [25], and deuteron [42]. Applying LSCA to Eq. (1), one obtains the DWIA T -matrix with LSCA [25] as

$$T^{\text{LSCA}} = \int d\mathbf{R} F(\mathbf{R}) \varphi_d(\mathbf{R}) \tilde{t}_{pd}(\boldsymbol{\kappa}(\mathbf{R}), \boldsymbol{\kappa}'(\mathbf{R})), \quad (3)$$

$$F(\mathbf{R}) \equiv \chi_1^{*(-)}(\mathbf{R}) \chi_2^{*(-)}(\mathbf{R}) \chi_0^{(+)}(\mathbf{R}) e^{-i\mathbf{K}_0(\mathbf{R}) \cdot \mathbf{R} A_d/A}, \quad (4)$$

$$\tilde{t}_{pd}(\boldsymbol{\kappa}(\mathbf{R}), \boldsymbol{\kappa}'(\mathbf{R})) \equiv \int ds e^{-i\boldsymbol{\kappa}'(\mathbf{R}) \cdot \mathbf{s}} t_{pd}(s) e^{i\boldsymbol{\kappa}(\mathbf{R}) \cdot \mathbf{s}}, \quad (5)$$

where $\boldsymbol{\kappa}(\mathbf{R})$ and $\boldsymbol{\kappa}'(\mathbf{R})$ are the local p - d relative momentum in the initial and final states, respectively, which are given by

$$\boldsymbol{\kappa}(\mathbf{R}) \equiv \frac{A+1}{A} \frac{A_d}{A_d+1} \mathbf{K}_0(\mathbf{R}) - \frac{1}{A_d+1} \mathbf{K}_d(\mathbf{R}), \quad (6)$$

$$\boldsymbol{\kappa}'(\mathbf{R}) \equiv \frac{A_d}{A_d+1} \mathbf{K}_1(\mathbf{R}) - \frac{1}{A_d+1} \mathbf{K}_2(\mathbf{R}) \quad (7)$$

as discussed in Ref. [25]. A_d and A are the mass numbers of the deuteron and the target nucleus, respectively. \mathbf{K}_d is determined to satisfy the momentum conservation of the p - d system:

$$\mathbf{K}_d(\mathbf{R}) = \mathbf{K}_1(\mathbf{R}) + \mathbf{K}_2(\mathbf{R}) - \frac{A+1}{A} \mathbf{K}_0(\mathbf{R}). \quad (8)$$

In the numerical calculation of Eq. (3), in many cases, \tilde{t}_{pd} parameterized in momentum space has been used, rather than calculating the right-hand-side of Eq. (5). In other words, the integration over \mathbf{s} seems to be unnecessary in the numerical calculation. Because of this, sometimes Eq. (3) is referred to as the zero-range approximation. However, it is obvious from Eq. (5) that the finite-range nature of $t_{pd}(s)$ is explicitly taken into account. Furthermore, in DWIA with LSCA, the arguments of \tilde{t}_{pd} depend

on \mathbf{R} , which is not the case with DWIA with AMA as one sees from Eqs. (16) and (17) below. The \mathbf{R} dependence of \tilde{t}_{pd} can be understood that the original 6-dimensional nature is more respected than in DWIA with AMA. We will return to this point later.

In the calculation of the (p, pd) cross section, $|T^{\text{LSCA}}|^2$ is obviously given by

$$\begin{aligned} |T^{\text{LSCA}}|^2 &= \int d\mathbf{R} \tilde{t}_{pd}(\boldsymbol{\kappa}(\mathbf{R}), \boldsymbol{\kappa}'(\mathbf{R})) F(\mathbf{R}) \varphi_d(\mathbf{R}) \\ &\quad \times \int d\mathbf{R}' \tilde{t}_{pd}^*(\boldsymbol{\kappa}(\mathbf{R}'), \boldsymbol{\kappa}'(\mathbf{R}')) F^*(\mathbf{R}') \varphi_d^*(\mathbf{R}'). \end{aligned} \quad (9)$$

We make an additional approximation in Eq. (9) as

$$\begin{aligned} &\tilde{t}_{pd}(\boldsymbol{\kappa}(\mathbf{R}), \boldsymbol{\kappa}'(\mathbf{R})) \tilde{t}_{pd}^*(\boldsymbol{\kappa}(\mathbf{R}'), \boldsymbol{\kappa}'(\mathbf{R}')) \\ &\approx |\tilde{t}_{pd}(\boldsymbol{\kappa}(\mathbf{R}), \boldsymbol{\kappa}'(\mathbf{R})) \tilde{t}_{pd}^*(\boldsymbol{\kappa}(\mathbf{R}'), \boldsymbol{\kappa}'(\mathbf{R}'))|, \end{aligned} \quad (10)$$

which assumes that the phases of $\tilde{t}_{pd}(\boldsymbol{\kappa}(\mathbf{R}), \boldsymbol{\kappa}'(\mathbf{R}))$ and $\tilde{t}_{pd}^*(\boldsymbol{\kappa}(\mathbf{R}'), \boldsymbol{\kappa}'(\mathbf{R}'))$ cancel out. A detailed discussion on this approximation is made in Appendix A.

Making the on-the-energy-shell (on-shell) approximation to \tilde{t}_{pd} using the relative momentum and the energy in the final state (final-state prescription), one obtains

$$\left(\frac{\mu_{pd}}{2\pi\hbar^2}\right)^2 |\tilde{t}_{pd}(\boldsymbol{\kappa}(\mathbf{R}), \boldsymbol{\kappa}'(\mathbf{R}))|^2 \approx \frac{d\sigma_{pd}}{d\Omega_{pd}}(\theta_{pd}(\mathbf{R}), E_{pd}(\mathbf{R})), \quad (11)$$

where μ_{pd} is the reduced energy of the p - d system and $d\sigma_{pd}/d\Omega_{pd}$ represents the p - d elastic cross section. The reduced T -matrix with LSCA is obtained as

$$\bar{T}^{\text{LSCA}} = \int d\mathbf{R} \sqrt{\frac{d\sigma_{pd}}{d\Omega_{pd}}(\theta_{pd}(\mathbf{R}), E_{pd}(\mathbf{R}))} F(\mathbf{R}) \varphi_d(\mathbf{R}). \quad (12)$$

The p - d scattering angle $\theta_{pd}(\mathbf{R})$ and the scattering energy $E_{pd}(\mathbf{R})$ are determined locally. Using \bar{T}^{LSCA} , the triple differential cross section (TDX) of the (p, pd) reaction is given by [3, 7, 52, 53]

$$\begin{aligned} \frac{d^3\sigma_{\text{LSCA}}^{\text{L}}}{dE_1^{\text{L}} d\Omega_1^{\text{L}} d\Omega_2^{\text{L}}} &= \frac{(2\pi)^4}{\hbar v} S_d F_{\text{kin}}^{\text{L}} \frac{E_1 E_2 E_B}{E_1^{\text{L}} E_2^{\text{L}} E_B^{\text{L}}} \frac{1}{2l+1} \\ &\quad \times \left(\frac{2\pi\hbar^2}{\mu_{pd}}\right)^2 |\bar{T}^{\text{LSCA}}|^2, \end{aligned} \quad (13)$$

$$F_{\text{kin}}^{\text{L}} \equiv \frac{E_1^{\text{L}} K_1^{\text{L}} E_2^{\text{L}} K_2^{\text{L}}}{(\hbar c)^2} \left[1 + \frac{E_2^{\text{L}}}{E_B^{\text{L}}} + \frac{E_2^{\text{L}}}{E_B^{\text{L}}} \frac{\mathbf{K}_X^{\text{L}} \cdot \mathbf{K}_2^{\text{L}}}{(K_2^{\text{L}})^2} \right]^{-1}, \quad (14)$$

with $\mathbf{K}_X^{\text{L}} = \mathbf{K}_1^{\text{L}} - \mathbf{K}_0^{\text{L}} - \mathbf{K}_A^{\text{L}}$. Here, Ω_i is the solid angle of \mathbf{K}_i of particle i . v is the relative velocity between particle 0 and the target A, l is the relative angular momentum between B and the deuteron in A. S_d is the

forementioned deuteron spectroscopic factor. As discussed in Sec. III A, only the $l = 0$ case is discussed in the present work.

In AMA [7, 25], $\mathbf{K}_i(\mathbf{R})$ is replaced with its asymptotic momentum \mathbf{K}_i . Thus, θ_{pd} , E_{pd} , and the p - d elementary cross section are determined only by the asymptotic momenta as

$$\left(\frac{\mu_{pd}}{2\pi\hbar^2}\right)^2 |\tilde{t}_{pd}(\boldsymbol{\kappa}, \boldsymbol{\kappa}')|^2 \approx \frac{d\sigma_{pd}}{d\Omega_{pd}}(\theta_{pd}, E_{pd}). \quad (15)$$

In other words, $d\sigma_{pd}/d\Omega_{pd}$ no longer depends on \mathbf{R} . The factorized form of the DWIA TDX is given by [3, 7, 52, 53]

$$\begin{aligned} \frac{d^3\sigma_{\text{AMA}}^{\text{L}}}{dE_1^{\text{L}} d\Omega_1^{\text{L}} d\Omega_2^{\text{L}}} &= \frac{(2\pi)^4}{\hbar v} S_d F_{\text{kin}}^{\text{L}} \frac{E_1 E_2 E_B}{E_1^{\text{L}} E_2^{\text{L}} E_B^{\text{L}}} \frac{1}{2l+1} \\ &\quad \times \left(\frac{2\pi\hbar^2}{\mu_{pd}}\right)^2 \frac{d\sigma_{pd}}{d\Omega_{pd}} |\bar{T}^{\text{AMA}}|^2, \end{aligned} \quad (16)$$

$$\bar{T}^{\text{AMA}} = \int d\mathbf{R} F(\mathbf{R}) \varphi_d(\mathbf{R}). \quad (17)$$

In this article, we call this the factorized form of the DWIA, not the zero-range DWIA (ZR-DWIA), because the p - d elastic cross section $d\sigma_{pd}/d\Omega_{pd}$ results from the p - d effective interaction $t_{pd}(\mathbf{s})$ as seen in Eqs. (5) and (15), which is a finite-range interaction. It should be noted, however, that as discussed in Sec. III A, we directly use experimental data of the p - d elastic cross section for $d\sigma_{pd}/d\Omega_{pd}$ in Eqs. (12) and (16). Therefore, an explicit form of $t_{pd}(\mathbf{s})$ is not considered in the present study.

III. RESULT AND DISCUSSION

A. Numerical input

The differential cross section of the p - d elastic scattering is prepared numerically by fitting the experimental data from 5 MeV to 800 MeV with respect to the scattering energy and the angle as shown in Fig. 2. The experimental data of the p - d elastic scattering are taken from Refs. [55–64]. The function used in the fitting is

$$\frac{d\sigma_{pd}}{d\Omega_{pd}} = \sum_{j=1}^{j_{\text{max}}} a_j \exp \left[- \left(\frac{\theta_{pd} - c_j}{b_j} \right)^2 \right] + d_0, \quad (18)$$

where j_{max} is 2 for 5–20 MeV, 3 for 35–250 MeV, and 4 for 425–800 MeV. All the parameters a_j , b_j , c_j , and d_0 are listed in Table I. It should be noted that c_1 ($c_{j_{\text{max}}}$) is fixed at 0° (180°). In the present calculation, the fitted p - d elastic cross section is interpolated to the required energy and scattering angle. Compared to the previous analysis [47] in which only the p - d scattering data at 22, 35, and 46 MeV [56] are used, the wide coverage of the p - d scattering energies improves the reliability

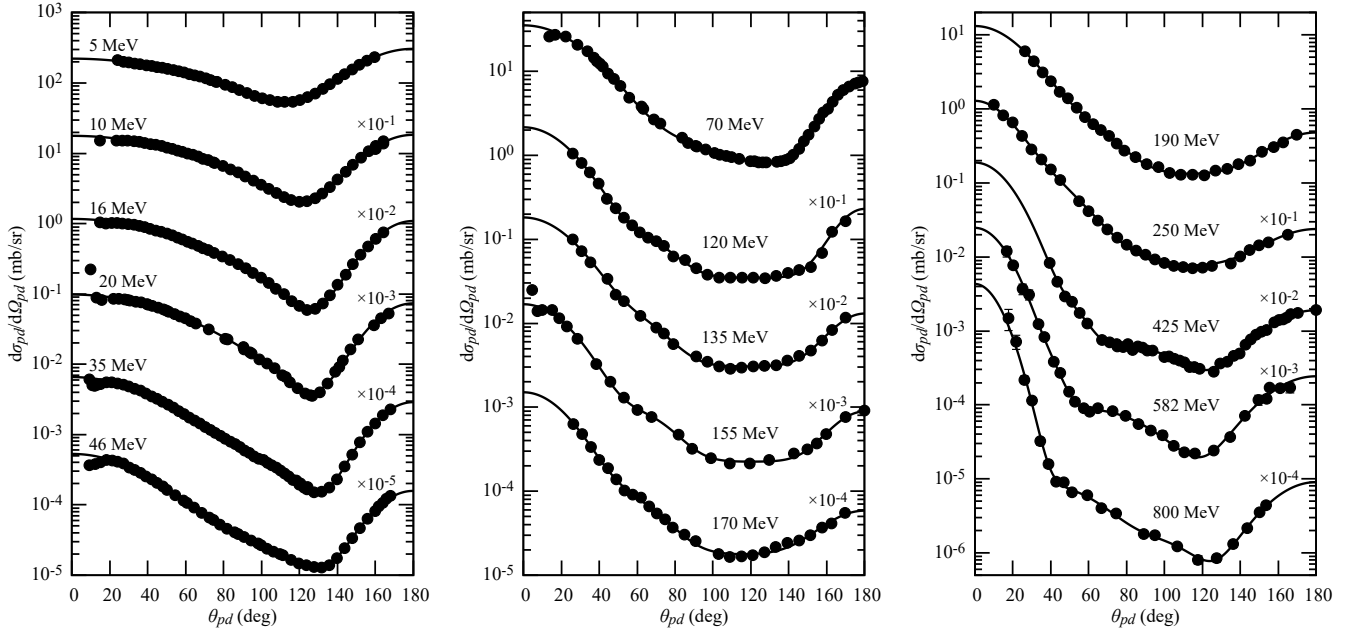


FIG. 2. Angular distribution of the p - d elastic scattering cross section. The horizontal axis is the center-of-mass scattering angle of the p - d system. The experimental data taken from Refs. [55–64] are represented by filled circles. The solid lines show the results of the fitting. See Eq. (18) and Table I for details.

of the elementary cross section of the (p, pd) reaction at $E_{pd} > 46$ MeV.

The proton distorted waves, χ_0 and χ_1 , are obtained as scattering waves under the phenomenological optical potential by Koning and Delaroche [65]. For the deuteron distorted wave χ_2 , the optical potential proposed by An and Cai [66] is adopted. The nonlocality correction to the distorted waves is taken into account by the Perey factor [67] with the range parameter $\beta = 0.85$ fm for the proton and $\beta = 0.54$ fm for the deuteron [68].

φ_d is obtained as a bound state wave function under the Woods-Saxon shaped potential with the range parameter $R_0 = 1.41 \times 14^{1/3}$ fm and the diffuseness parameter $a_0 = 0.65$ fm [47]. The depth parameter of the potential is adjusted to reproduce the effective deuteron separation energy of 24.7 MeV, which is the sum of the deuteron separation energy of ^{16}O (20.74 MeV) and the excitation energy of the ^{14}N residue (3.95 MeV). As discussed in Ref. [47], the $^{16}\text{O}(p, pd)^{14}\text{N}_{1+}$ data show a typical s -wave peak at the recoilless condition, in which the reaction residue is at rest in the final state. Following Ref. [47], we only consider $l = 0$ for the d - $^{14}\text{N}_{1+}$ relative angular momentum.

B. Refraction effect in $^{16}\text{O}(p, pd)^{14}\text{N}$

The TDXs of the $^{16}\text{O}(p, pd)^{14}\text{N}_{1+}$ at 101.3 MeV calculated with LSCA and AMA, and the experimental data [47] are shown in Fig. 3 as a function of the proton

emission energy T_1^L . The proton and deuteron emission

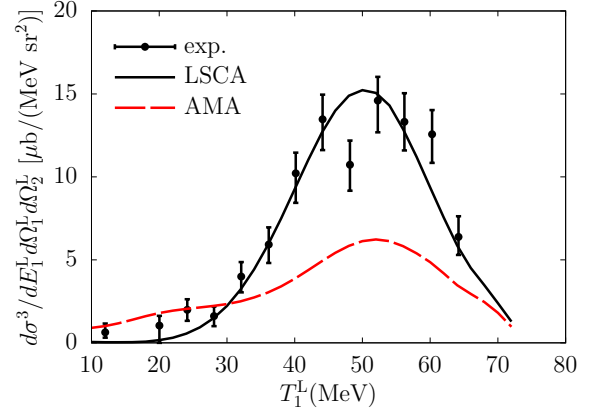


FIG. 3. TDXs of the $^{16}\text{O}(p, pd)^{14}\text{N}_{1+}$ reaction calculated with LSCA and AMA in comparison with the experimental data [47]. Both are multiplied by $S_d = 1.74$.

angles are $\theta_1^L = 40.1^\circ$ and $\theta_2^L = 40.0^\circ$, respectively, and the kinematics are in coplanar. The TDX with LSCA clearly shows better agreement with the data than that with AMA in their shape, showing that the refraction effect is important. The experimental spectroscopic factor $S_d = 1.74$ is obtained by fitting the theoretical curve of LSCA to the data. The TDX using AMA is also multiplied by $S_d = 1.74$ for comparison. The obtained S_d is consistent with the $1p$ shell model prediction at early ages [69] $S_d = 1.75$, which is referred in the former ex-

E_{pd}	j	a_j	b_j	c_j	d_0
5	1	222.1560	86.8088	0.0000	0.0000
	2	302.8700	37.5459	180.0000	
10	1	177.2360	78.7301	0.0000	0.0000
	2	182.1080	30.6876	180.0000	
16	1	116.5830	70.8749	0.0000	0.0000
	2	108.7870	26.0295	180.0000	
20	1	97.9835	67.8439	0.0000	0.0000
	2	73.3261	25.8404	180.0000	
35	1	65.6339	52.7178	0.0000	0.0000
	2	2.7094	35.3458	93.5447	
	3	28.8682	24.2590	180.0000	
46	1	52.7869	44.5933	0.0000	0.0000
	2	2.7551	48.1972	80.0000	
	3	15.7479	24.9981	180.0000	
70	1	34.6225	38.2736	0.0000	0.7461
	2	0.5250	29.8396	80.0000	
	3	6.9138	21.1479	180.0000	
120	1	21.2430	30.7048	0.0000	0.3485
	2	0.4932	19.8301	64.7798	
	3	1.9542	18.4435	180.0000	
135	1	17.8934	31.7476	0.0000	0.3064
	2	0.5316	20.8098	61.0116	
	3	0.9988	21.4401	180.0000	
155	1	16.6284	29.5589	0.0000	0.2246
	2	0.4812	20.5405	63.6499	
	3	0.6649	21.1364	180.0000	
170	1	14.8897	27.9947	0.0000	0.1761
	2	0.5273	23.9095	55.2300	
	3	0.4100	26.4076	180.0000	
190	1	13.0640	28.5562	0.0000	0.1305
	2	0.5110	26.0810	50.0000	
	3	0.3499	28.3901	180.0000	
250	1	9.6172	20.2655	0.0000	0.0741
	2	3.1887	40.5310	0.0000	
	3	0.1642	30.3782	180.0000	
425	1	18.8803	21.7724	0.0000	0.1305
	2	0.1294	13.0634	49.2562	
	3	0.0613	38.2106	80.0000	
	4	0.1900	34.5092	180.0000	
582	1	24.7257	18.9076	0.0000	0.1305
	2	0.1519	10.1242	38.0159	
	3	0.0858	41.6712	60.0000	
	4	0.2437	33.0826	180.0000	
800	1	43.1368	15.4699	0.0000	0.1305
	2	0.0780	33.9306	40.0000	
	3	0.0111	25.3878	100.0000	
	4	0.0904	30.4011	180.0000	

TABLE I. Numerical value of the parameters in Eq. (18). E_{pd} is given in MeV, a_j and d_0 are in mb/sr, θ_{pd} , b_j , and c_j are in degrees.

perimental analyses [47, 70], and is comparable with 1.43 determined in the ZR-DWIA analysis [51].

As discussed in Sec. II, LSCA should partially incorporate the finite-range nature of the p - d effective interaction

into the p - d cross section through the \mathbf{R} dependence of $\kappa(\mathbf{R})$ and $\kappa'(\mathbf{R})$. As seen in the difference between the LSCA and AMA results in Fig. 3, the shape of the distribution strongly depend on how θ_{pd} and E_{pd} are evaluated. The present analysis shows that LSCA is valid for reproducing both the shape and the height of the experimental data and the cross section with a reasonable S_d as long as $d\sigma_{pd}/d\Omega_{pd}$ is prepared precisely as in Fig. 2.

The origin of the inconsistency between the present AMA and the ZR-DWIA in Ref. [51] is not clear. In the present AMA calculation, the shape of the TDX cannot be reproduced as shown in Fig. 3, while the ZR-DWIA calculation gives good agreement with the data as shown in Fig. 2 of Ref. [51]. Although the detail of the ZR-DWIA calculation is not described in Ref. [51], the inconsistency may arise from the different treatment of the p - d elementary process. In the present study we use the fitted function of the experimental p - d differential cross sections as shown in Fig. 2, while in Ref. [51] they constructed $t_{pd}(\mathbf{s})$ (denoted as $t_L(E, r)$ in the reference) based on the p - d optical potential [56, 71, 72]. Also the difference between the present LSCA result and the FR-DWIA in Ref. [51] is not clear. In two types of the FR-DWIA analysis in Ref. [51], all attractive and repulsive core, $S_d = 0.47$ and 0.12 are obtained, respectively, which are both smaller than the present value of 1.74, suggesting again that the difference in the treatment of the p - d elementary process. It should be noted here that the diffraction effect should be naturally implemented in FR-DWIA by the explicit distance-dependent p - d t -matrix and the 6-dimensional integral. The AMA formalism of the present work is essentially identical to that used in the analysis of the original experimental data [47]. The inconsistency between the present AMA result and the curve in Fig. 2. (a) of Ref. [47] is found to be due to the differences in the optical potentials and the p - d cross section used as inputs. Details are discussed in Appendix B.

To investigate the impact of the deuteron refraction at higher energies, we consider the same reaction at 250 MeV; the results are shown in Fig. 4. The kinematics conditions are fixed at $\theta_1^L = 47.1^\circ$ and $\theta_2^L = 48.8^\circ$, which gives the recoilless condition at around $T_1^L = 150$ MeV. Since there is no experimental data at higher energies, only the theoretical curves are shown assuming $S_d = 1$ in Fig. 4. It is clearly shown that the result using LSCA is almost equivalent to that using AMA at 250 MeV, in contrast to the 101.3 MeV case in Fig. 3. This result is consistent with the previous work on the $^{120}\text{Sn}(p, p\alpha)^{116}\text{Cd}$ reaction at 392 MeV [25].

IV. SUMMARY

The refraction effect on the elementary process of the (p, pd) reaction has been investigated by using LSCA in the DWIA framework. It is found that the effect gives a significant change in the shape of the energy sharing

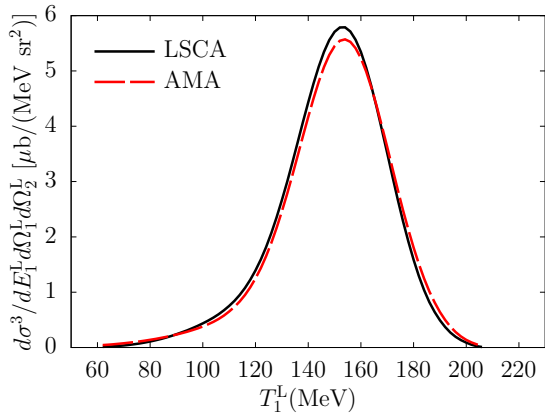


FIG. 4. Same as Fig. 3 but at 250 MeV.

distribution of the $^{16}\text{O}(p,pd)^{14}\text{N}$ reaction at 101.3 MeV. The present analysis using LSCA gives $S_d = 1.74$, which is consistent with $1p$ shell model prediction 1.75 [69] referred in Refs. [47, 70], and comparable with 1.43 by the previous ZR-DWIA analysis [51]. On the other hand, at 250 MeV, the results with LSCA and AMA are similar, showing that the local p - d kinematics has little effect on the TDX and the commonly used factorized form of the DWIA with AMA can be safely applied to the reaction analysis at this energy.

As discussed in Refs. [41, 53], the description of the spatial distribution and the radial magnitude of $\varphi_d(\mathbf{R})$ based on microscopic structure theories is still challenging but important for the quantitative discussion of the deuteron-like p - n pair in nuclei. A combination of the present work and CDCCIA [41], which takes into account the breakup and the reformation process of the p - n pair, will be important for the accurate description of the (p,pd) reaction. The development of such framework as well as a numerical code is ongoing.

ACKNOWLEDGMENTS

We thank T. Uesaka and S. Ogawa for fruitful discussions. This work is supported in part by Grants-in-Aid for Scientific Research from the JSPS (Grants No. JP20K14475, JP21H00125, and JP21H04975).

Appendix A: Local cross section approximation

Equation (10) assumes the cancellation of the complex phase factors of $\tilde{t}_{pd}(\boldsymbol{\kappa}(\mathbf{R}), \boldsymbol{\kappa}'(\mathbf{R}))$ and $\tilde{t}_{pd}^*(\boldsymbol{\kappa}(\mathbf{R}'), \boldsymbol{\kappa}'(\mathbf{R}'))$. In this Appendix we consider this approximation in terms of $t_{pd}(\mathbf{s})$, the effective interaction in the coordinate space. Here, we assume that $t_{pd}(\mathbf{s})$ is the p - d effective interaction parameterized so as to reproduce the p - d elastic cross

section only with the central term:

$$t_{pd}(E, \mathbf{s}) = [v(E) + iw(E)] f(s), \quad (\text{A1})$$

with E being the incident energy, and $v(E)$ and $w(E)$ are the energy dependent real and imaginary part of the central term strength. To show the energy dependence of t_{pd} clearly, E is added to its argument. The radial dependence of the effective interaction is expressed by the real function $f(s)$. The Fourier transform of Eq. (A1) is given by

$$\tilde{t}_{pd}(E, q) = [v(E) + iw(E)] \tilde{f}(q), \quad (\text{A2})$$

$$\tilde{f}(q) \equiv 4\pi \int j_0(qs) f(s) s^2 ds, \quad (\text{A3})$$

where \mathbf{q} is the conjugate momentum of the coordinate \mathbf{s} , and j_0 is the zeroth spherical Bessel function.

Using Eq. (A2) with $\mathbf{q}(\mathbf{R}) \equiv \boldsymbol{\kappa}(\mathbf{R}) - \boldsymbol{\kappa}'(\mathbf{R})$, the left- and the right-hand sides of Eq. (10) are rewritten as

$$\begin{aligned} & \tilde{t}_{pd}(\boldsymbol{\kappa}(\mathbf{R}), \boldsymbol{\kappa}'(\mathbf{R})) \tilde{t}_{pd}^*(\boldsymbol{\kappa}(\mathbf{R}'), \boldsymbol{\kappa}'(\mathbf{R}')) \\ &= \tilde{t}_{pd}(E, \mathbf{q}(\mathbf{R})) \tilde{t}_{pd}^*(E', \mathbf{q}(\mathbf{R}')) \\ &= [v(E) + iw(E)] [v(E') - iw(E')] \\ & \quad \times \tilde{f}(\mathbf{q}(\mathbf{R})) \tilde{f}(\mathbf{q}(\mathbf{R}')) \end{aligned} \quad (\text{A4})$$

and

$$\begin{aligned} & |\tilde{t}_{pd}(\boldsymbol{\kappa}(\mathbf{R}), \boldsymbol{\kappa}'(\mathbf{R})) \tilde{t}_{pd}^*(\boldsymbol{\kappa}(\mathbf{R}'), \boldsymbol{\kappa}'(\mathbf{R}'))| \\ &= \sqrt{v^2(E) + w^2(E)} \sqrt{v^2(E') + w^2(E')} \\ & \quad \times \tilde{f}(\mathbf{q}(\mathbf{R})) \tilde{f}(\mathbf{q}(\mathbf{R}')), \end{aligned} \quad (\text{A5})$$

respectively. Thus, the approximation of Eq. (10) implies

$$v(E) + iw(E) \approx v(E') + iw(E'), \quad (\text{A6})$$

that the energy dependence of \tilde{t}_{pd} through $v(E)$ and $w(E)$ is negligible for different \mathbf{R} , compared to the $\mathbf{q}(\mathbf{R})$ dependence. It should be noted that no approximation is made to $\tilde{f}(\mathbf{q}(\mathbf{R}))$ or $\tilde{f}(\mathbf{q}(\mathbf{R}'))$. Therefore, the angular dependence of \tilde{t}_{pd} is taken into account properly in this approximation. In the present study, this approximation is expected to be good since the energy dependence of the p - d elastic cross section is weak compared to its angular dependence, as shown in Fig. 2.

Appendix B: On discrepancy between Samanta *et al.* and the present analysis

The theoretical frameworks of the present AMA result (see Fig. 3 of the present work) and the curve in Fig. 2 (a) of Ref. [47] are essentially the same, but a clear discrepancy can be seen in these results, in both shape of the TDX and the extracted $S_d = 1.74$ and 0.43. In this Appendix, we show that the discrepancy is due to the differences in the p - d elastic cross section and the optical potentials used as the inputs in these analyses.

In the previous analysis in Ref. [47], the p - d elastic scattering cross section data at 22, 35, and 46 MeV [56] were used, as mentioned in Sec. III A of the present paper. By the AMA analysis of the present work, it was found that in the $^{16}\text{O}(p,pd)^{14}\text{N}$ kinematics of Fig. 3 of the present work and Fig. 2 (a) of Ref. [47], the referred p - d scattering energy ranges $35 \lesssim E_{pd} \lesssim 70$ MeV, which increases monotonically with increasing T_1^L . At $T_1^L \sim 35$ MeV, E_{pd} exceeds 46 MeV and thus the p - d cross section is extrapolated in $T_1^L \gtrsim 35$ MeV, if the p - d cross section data at 22, 35, and 46 MeV are used.

For the optical potentials, in the previous analysis of Ref. [47], the parameter set determined from the p - ^{12}C scattering at 100 MeV [73] and 75 MeV [74] are adopted for the initial p - ^{16}O and the final p - ^{14}N distorted waves, respectively. For the d - ^{14}N in the final channel, the d - ^{14}N optical potential parameters determined at 28 MeV [75] are used. Due to the difference in the available data and the optical potential parameters, we found that the result differs from that obtained with the modern input in the present study.

In Fig. 5, we show the AMA results calculated with the optical potentials and the p - d cross section used in the earlier work by Samanta *et al.* [47] as mentioned above. Note that $S_d = 0.43$ from Samanta *et al.* [47] is applied

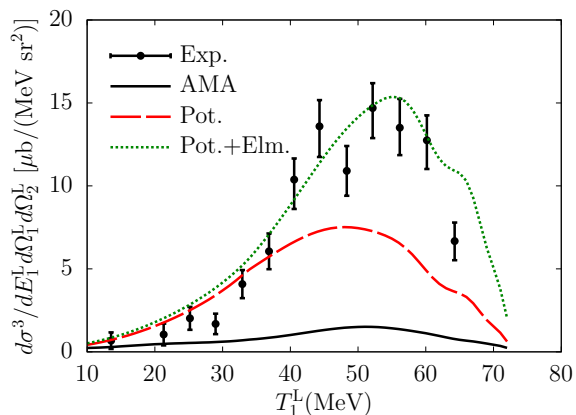


FIG. 5. Comparison of AMA TDXs of the present work and that using the inputs and $S_d = 0.43$ of Samanta *et al.* [47]. The solid line is the AMA result of the present work (same as the dashed line in Fig. 3 but with $S_d = 0.43$), the dashed line shows the same calculation but using the optical potentials used Samanta *et al.* The dotted line shows the AMA calculations using both the optical potentials and the p - d cross section used in Samanta *et al.*

to all curves in Fig. 5 for comparison. The dashed line in Fig. 5 shows the AMA result using the optical potentials used in Samanta *et al.* [47]. One sees a remarkable increase of the TDX compared to the present AMA result (solid line), while the shape of the curve remains similar. It is found that the changes in the p - ^{16}O , p - ^{14}N , and d - ^{14}N potentials cause a change in the height of the TDX by factors of 1.2, 2.0, and 2.2, respectively. Furthermore, using the p - d cross section which is adopted in Ref. [47], we obtain the TDX as shown by the dotted line in Fig. 5. It can also be seen that the difference in the p - d cross section changes both the magnitude and the shape of the TDX. In particular, the shape changes in $T_1^L \gtrsim 35$ MeV, indicating that the extrapolation beyond $E_{pd} = 46$ MeV makes the difference. The agreement in shape with the experimental data around the peak seems rather coincidental, since the energy and angular dependence of the p - d cross section should be better described in the present work. The dotted line in Fig. 5 of the present work is almost identical to Fig. 2 (a) of Ref. [47], and it can be concluded that the difference between the present AMA result and the DWIA calculation in Ref. [47] originates from the differences of the optical potentials and the p - d cross section used as the inputs.

-
- [1] G. Jacob and T. A. J. Maris, Quasi-Free Scattering and Nuclear Structure, *Rev. Mod. Phys.* **38**, 121 (1966).
 [2] G. Jacob and T. A. J. Maris, Quasi-Free Scattering and Nuclear Structure. II., *Rev. Mod. Phys.* **45**, 6 (1973).
 [3] N. S. Chant and P. G. Roos, Distorted-wave impulse-approximation calculations for quasifree cluster knockout

- reactions, *Phys. Rev. C* **15**, 57 (1977).
 [4] N. S. Chant and P. G. Roos, Spin orbit effects in quasifree knockout reactions, *Phys. Rev. C* **27**, 1060 (1983).
 [5] P. Kitching, W. J. McDonald, T. A. J. Maris, and C. A. Z. Vasconcellos, Recent Developments in Quasi-Free Nucleon-Nucleon Scattering, in *Advances in Nuclear*

- Physics*, edited by J. W. Negele and E. Vogt (Springer US, Boston, MA, 1985) pp. 43–83.
- [6] A. A. Cowley, J. J. Lawrie, G. C. Hillhouse, D. M. Whittal, S. V. Förtsch, J. V. Pilcher, F. D. Smit, and P. G. Roos, Quasifree knockout in $^{16}\text{O}(p,2p)^{15}\text{N}$ at an incident energy of 151 MeV, *Phys. Rev. C* **44**, 329 (1991).
- [7] T. Wakasa, K. Ogata, and T. Noro, Proton-induced knockout reactions with polarized and unpolarized beams, *Prog. Part. Nucl. Phys.* **96**, 32 (2017).
- [8] T. Noro, T. Wakasa, T. Ishida, H. P. Yoshida, M. Dozono, H. Fujimura, K. Fujita, K. Hatanaka, T. Ishikawa, M. Itoh, J. Kamiya, T. Kawabata, Y. Maeda, H. Matsubara, M. Nakamura, H. Sakaguchi, Y. Sakemi, Y. Shimizu, H. Takeda, Y. Tameshige, A. Tamii, K. Tamura, S. Terashima, M. Uchida, Y. Yasuda, and M. Yosoi, Experimental study of $(p,2p)$ reactions at 392 MeV on ^{12}C , ^{16}O , ^{40}Ca and ^{208}Pb nuclei leading to low-lying states of residual nuclei, *Prog. Theor. Exp. Phys.* **2020**, 093D02 (2020).
- [9] T. Noro, S. Sakaguchi, T. Wakasa, M. Dozono, H. Fujioka, K. Fujita, K. Hatanaka, T. Ishida, C. Iwamoto, S. Kawase, Y. Kubota, Y. Maeda, H. Matsubara, K. Miki, S. Ota, V. Panin, H. Sakaguchi, A. Sakae, Y. Sakemi, M. Sasano, K. Sekiguchi, Y. Shimizu, H. Takeda, Y. Tameshige, A. Tamii, S. Terashima, T. Uesaka, Z.-H. Yang, Y. Yasuda, H. P. Yoshida, and J. Zenihiro, Experimental study of $(p,2p)$ reactions at 197 MeV on ^{12}C , ^{16}O , $^{40,48}\text{Ca}$, and ^{90}Zr nuclei leading to low-lying states of residual nuclei, *Prog. Theor. Exp. Phys.* **2023**, 093D01 (2023).
- [10] B. Gottschalk and S. L. Kannenberg, Quasi-Elastic Scattering of 160-MeV Protons by Alpha Clusters in Light Nuclei. I. Carbon, *Phys. Rev. C* **2**, 24 (1970).
- [11] D. Bachelier, M. Bernas, O. M. Bilaniuk, J. L. Boyard, J. C. Jourdain, and P. Radvanyi, Quasifree $(p,p\alpha)$ Scattering on ^6Li , ^{24}Mg , ^{28}Si , ^{40}Ca , ^{140}Ce , and ^{232}Th at 156 MeV, *Phys. Rev. C* **7**, 165 (1973).
- [12] D. Bachelier, J. Boyard, T. Hennino, H. Holmgren, J. Jourdain, P. Radvanyi, P. Roos, and M. Roy-Stephan, Quasi-free $(p,p\alpha)$ scattering on ^{24}Mg , ^{28}Si , ^{40}Ca and ^{58}Ni at 157 MeV, *Nucl. Phys. A* **268**, 488 (1976).
- [13] P. G. Roos, N. S. Chant, A. A. Cowley, D. A. Goldberg, H. D. Holmgren, and R. Woody, Absolute spectroscopic factors from the $(p,p\alpha)$ reaction at 100 MeV on $1p$ -shell nuclei, *Phys. Rev. C* **15**, 69 (1977).
- [14] G. Landaud, A. Devaux, P. Delpierre, J. Kahane, R. Sené, J. Yonnet, and R. Anne, Quasielastic knockout of alpha clusters from light and medium nuclei by 600 MeV protons, *Phys. Rev. C* **18**, 1776 (1978).
- [15] A. Nadasen, N. S. Chant, P. G. Roos, T. A. Carey, R. Cowen, C. Samanta, and J. Wesick, Non-coplanar $(p,p\alpha)$ and $(p,d^3\text{He})$ reactions on ^9Be at 101.5 MeV, *Phys. Rev. C* **22**, 1394 (1980).
- [16] T. A. Carey, P. G. Roos, N. S. Chant, A. Nadasen, and H. L. Chen, Alpha-clustering systematics from the quasifree $(p,p\alpha)$ knockout reaction, *Phys. Rev. C* **23**, 576 (1981).
- [17] T. A. Carey, P. G. Roos, N. S. Chant, A. Nadasen, and H. L. Chen, Alpha-particle spectroscopic strengths using the $(p,p\alpha)$ reaction at 101.5 MeV, *Phys. Rev. C* **29**, 1273 (1984).
- [18] C. W. Wang, P. G. Roos, N. S. Chant, G. Ciangaru, F. Khazaie, D. J. Mack, A. Nadasen, S. J. Mills, R. E. Warner, E. Norbeck, F. D. Becchetti, J. W. Janecke, and P. M. Lister, $^9\text{Be}(p,p\alpha)^5\text{He}$ cluster knockout reaction with 150 MeV polarized protons, *Phys. Rev. C* **31**, 1662 (1985).
- [19] A. Nadasen, P. G. Roos, N. S. Chant, C. C. Chang, G. Ciangaru, H. F. Breuer, J. Wesick, and E. Norbeck, $(p,p\alpha)$ cluster-knockout reaction on ^9Be at 200 MeV, *Phys. Rev. C* **40**, 1130 (1989).
- [20] T. Yoshimura, A. Okihana, R. Warner, N. Chant, P. Roos, C. Samanta, S. Kakigi, N. Koori, M. Fujiwara, N. Matsuoka, K. Tamura, E. Kubo, and K. Ushiro, Alpha spectroscopic factors for ^6Li , ^7Li , ^9Be and ^{12}C from the $(p,p\alpha)$ reaction at 296 MeV, *Nucl. Phys. A* **641**, 3 (1998).
- [21] R. Neveling, A. A. Cowley, Z. Buthelezi, S. V. Förtsch, H. Fujita, G. C. Hillhouse, J. J. Lawrie, G. F. Steyn, F. D. Smit, S. M. Wyngaardt, N. T. Botha, L. Mudau, and S. S. Ntshangase, Analyzing power of the $^{40}\text{Ca}(\bar{p},p\alpha)$ reaction at 100 MeV, *Phys. Rev. C* **77**, 037601 (2008).
- [22] A. A. Cowley, J. Mabiala, E. Z. Buthelezi, S. V. Förtsch, R. Neveling, F. D. Smit, G. F. Steyn, and J. J. van Zyl, Analyzing power distribution in the $^{12}\text{C}(p,p\alpha)^8\text{Be}(g.s.)$ reaction at an incident energy of 100 MeV, *Europhysics Letters* **85**, 22001 (2009).
- [23] J. Mabiala, A. A. Cowley, S. V. Förtsch, E. Z. Buthelezi, R. Neveling, F. D. Smit, G. F. Steyn, and J. J. Van Zyl, Analyzing power and cross section distributions of the $^{12}\text{C}(p,p\alpha)^8\text{Be}$ cluster knockout reaction at an incident energy of 100 MeV, *Phys. Rev. C* **79**, 054612 (2009).
- [24] S. Typel, Neutron skin thickness of heavy nuclei with α -particle correlations and the slope of the nuclear symmetry energy, *Phys. Rev. C* **89**, 064321 (2014).
- [25] K. Yoshida, K. Minomo, and K. Ogata, Investigating α clustering on the surface of ^{120}Sn via the $(p,p\alpha)$ reaction, and the validity of the factorization approximation, *Phys. Rev. C* **94**, 044604 (2016).
- [26] M. Lyu, K. Yoshida, Y. Kanada-En'yo, and K. Ogata, Manifestation of α clustering in ^{10}Be via α -knockout reaction, *Phys. Rev. C* **97**, 044612 (2018).
- [27] K. Yoshida, K. Ogata, and Y. Kanada-En'yo, Investigation of α clustering with knockout reactions, *Phys. Rev. C* **98**, 024614 (2018).
- [28] K. Yoshida, Y. Chiba, M. Kimura, Y. Taniguchi, Y. Kanada-En'yo, and K. Ogata, Quantitative description of the $^{20}\text{Ne}(p,p\alpha)^{16}\text{O}$ reaction as a means of probing the surface α amplitude, *Phys. Rev. C* **100**, 044601 (2019).
- [29] M. Lyu, K. Yoshida, Y. Kanada-En'yo, and K. Ogata, Direct probing of the cluster structure in ^{12}Be via the α -knockout reaction, *Phys. Rev. C* **99**, 064610 (2019).
- [30] A. A. Cowley, Sensitivity of analyzing power to distorting potentials in the quasifree reaction $^{40}\text{Ca}(p,p\alpha)^{36}\text{Ar}$ at 100 MeV incident energy: Comparison with ^9Be and ^{12}C targets, *Phys. Rev. C* **103**, 034622 (2021).
- [31] Y. Taniguchi, K. Yoshida, Y. Chiba, Y. Kanada-En'yo, M. Kimura, and K. Ogata, Unexpectedly enhanced α -particle preformation in ^{48}Ti probed by the $(p,p\alpha)$ reaction, *Phys. Rev. C* **103**, L031305 (2021).
- [32] J. Tanaka, Z. Yang, S. Typel, S. Adachi, S. Bai, P. van Beek, D. Beaumel, Y. Fujikawa, J. Han, S. Heil, S. Huang, A. Inoue, Y. Jiang, M. Knösel, N. Kobayashi, Y. Kubota, W. Liu, J. Lou, Y. Maeda, Y. Matsuda, K. Miki, S. Nakamura, K. Ogata, V. Panin, H. Scheit, F. Schindler, P. Schrock, D. Symochko, A. Tamii, T. Uesaka, V. Wagner, K. Yoshida, J. Zenihiro, and T. Au-

- mann, Formation of α clusters in dilute neutron-rich matter, *Science* **371**, 260 (2021).
- [33] K. Yoshida and J. Tanaka, α knockout reaction as a new probe for α formation in α -decay nuclei, *Phys. Rev. C* **106**, 014621 (2022).
- [34] T. Edagawa, K. Yoshida, Y. Chazono, and K. Ogata, Effective polarization in proton-induced α knockout reactions, *Phys. Rev. C* **107**, 054603 (2023).
- [35] S. Typel, Clusters in Nuclear Matter and the Equation of State, *Journal of Physics: Conference Series* **420**, 012078 (2013).
- [36] Z.-W. Zhang and L.-W. Chen, Low density nuclear matter with light clusters in a generalized nonlinear relativistic mean-field model, *Phys. Rev. C* **95**, 064330 (2017).
- [37] JSPS Grant-in-Aid for Specially Promoted Research “Comprehensive research of cluster formation in nuclear matter”, Tomohiro Uesaka, Kazuyuki Ogata, Juzo Zenihiro, and Shunsuke Kurosawa (2021–2026).
- [38] M. Kamimura, M. Yahiro, Y. Iseri, Y. Sakuragi, H. Kameyama, and M. Kawai, Chapter I. Projectile Breakup Processes in Nuclear Reactions, *Prog. Theor. Phys. Suppl.* **89**, 1 (1986).
- [39] N. Austern, Y. Iseri, M. Kamimura, M. Kawai, G. Rauscher, and M. Yahiro, Continuum-discretized coupled-channels calculations for three-body models of deuteron-nucleus reactions, *Physics Reports* **154**, 125 (1987).
- [40] M. Yahiro, K. Ogata, T. Matsumoto, and K. Minomo, The continuum discretized coupled-channels method and its applications, *Prog. Theor. Exp. Phys.* **2012**, 01A206 (2012).
- [41] Y. Chazono, K. Yoshida, and K. Ogata, Importance of deuteron breakup in the deuteron knockout reaction, *Phys. Rev. C* **106**, 064613 (2022).
- [42] H. Nakada, K. Yoshida, and K. Ogata, Description of the inclusive (d, d') reaction with the semiclassical distorted-wave model, *Phys. Rev. C* **108**, 034603 (2023).
- [43] Y. L. Luo and M. Kawai, Semiclassical distorted wave model of nucleon inelastic scattering to continuum, *Phys. Rev. C* **43**, 2367 (1991).
- [44] Y. Watanabe, R. Kuwata, S. Weili, M. Higashi, H. Shinohara, M. Kohno, K. Ogata, and M. Kawai, Semiclassical distorted wave model analysis of multistep direct ($p, p'x$) and (p, nx) reactions to the continuum, *Phys. Rev. C* **59**, 2136 (1999).
- [45] P. Kitching, W. C. Olsen, H. S. Sherif, W. Dollhopf, C. Lunke, C. F. Perdrisat, J. R. Priest, and W. K. Roberts, (p, pd) reaction on ${}^6\text{Li}$ at 590 MeV for high recoil momenta, *Phys. Rev. C* **11**, 420 (1975).
- [46] J. Erő, Z. Fodor, P. Koncz, Z. Seres, M. Csatlós, B. Khomenko, N. Khovanskij, Z. Krumstein, Y. Merekov, and V. Petrukhin, Quasi-free scattering in ${}^7\text{Li}(p, pd){}^5\text{He}$ and ${}^{12}\text{C}(p, pd){}^{10}\text{B}$ reactions at 670 MeV, *Nucl. Phys. A* **372**, 317 (1981).
- [47] C. Samanta, N. S. Chant, P. G. Roos, A. Nadasen, and A. A. Cowley, Discrepancy between proton- and alpha-induced cluster knockout reactions on ${}^{16}\text{O}$, *Phys. Rev. C* **26**, 1379 (1982).
- [48] R. Warner, J.-Q. Yang, D. Friesel, P. Schwandt, G. Caskey, A. Galonsky, B. Remington, A. Nadasen, N. Chant, F. Khazaie, and C. Wang, Comparison of the noncoplanar ${}^6\text{Li}(p, pd){}^4\text{He}$ reactions at 120 and 200 MeV, *Nucl. Phys. A* **443**, 64 (1985).
- [49] R. Warner, B. Vaughan, D. Friesel, P. Schwandt, J.-Q. Yang, G. Caskey, A. Galonsky, B. Remington, and A. Nadasen, The noncoplanar ${}^7\text{Li}(p, pd){}^5\text{He}$ and ${}^7\text{Li}(p, pt){}^4\text{He}$ reactions at $E_p = 200$ MeV, and evidence for deuteron clustering in ${}^7\text{Li}$, *Nucl. Phys. A* **453**, 605 (1986).
- [50] S. Terashima, L. Yu, H. J. Ong, I. Tanihata, S. Adachi, N. Aoi, P. Y. Chan, H. Fujioka, M. Fukuda, H. Geissel, G. Gey, J. Golak, E. Haettner, C. Iwamoto, T. Kawabata, H. Kamada, X. Y. Le, H. Sakaguchi, A. Sakaue, C. Scheidenberger, R. Skibiński, B. H. Sun, A. Tamii, T. L. Tang, D. T. Tran, K. Topolnicki, T. F. Wang, Y. N. Watanabe, H. Weick, H. Witała, G. X. Zhang, and L. H. Zhu, Dominance of Tensor Correlations in High-Momentum Nucleon Pairs Studied by (p, pd) Reaction, *Phys. Rev. Lett.* **121**, 242501 (2018).
- [51] B. N. Joshi, M. Kushwaha, and A. K. Jain, On the discrepancy between proton and α -induced d -cluster knockout on ${}^{16}\text{O}$, *Prog. Theor. Exp. Phys.* **2016**, 121D01 (2016).
- [52] K. Ogata, K. Yoshida, and Y. Chazono, pikoe: A computer program for distorted-wave impulse approximation calculation for proton induced nucleon knockout reactions, *Comput. Phys. Commun.* **297**, 109058 (2024).
- [53] Y. Chazono, K. Yoshida, K. Yoshida, and K. Ogata, Proton-induced deuteron knockout reaction as a probe of an isoscalar proton-neutron pair in nuclei, *Phys. Rev. C* **103**, 024609 (2021).
- [54] K. Minomo, K. Ogata, M. Kohno, Y. R. Shimizu, and M. Yahiro, Briefly-Rook localization of the microscopic nucleon-nucleus potential, *Journal of Physics G: Nuclear and Particle Physics* **37**, 085011 (2010).
- [55] K. Kuroda, A. Michalowicz, and M. Poulet, Mesure de la section efficace différentielle de diffusion proton-deuteron a 155 MeV, *Phys. Lett.* **13**, 67 (1964).
- [56] S. N. Bunker, J. M. Cameron, R. Carlson, J. R. Richardson, P. Tomáš, W. T. H. Van Oers, and J. W. Verba, Differential cross sections and polarizations in elastic p - d scattering at medium energies, *Nucl. Phys. A* **113**, 461 (1968).
- [57] T. A. Cahill, J. Greenwood, H. Willmes, and D. J. Shadoan, Elastic Scattering of Protons by Deuterium Between 15 and 20 MeV, *Phys. Rev. C* **4**, 1499 (1971).
- [58] N. E. Booth, C. Dolnick, R. J. Esterling, J. Parry, J. Scheid, and D. Sherden, Proton-Deuteron Elastic Scattering at 1.0 GeV/c, *Phys. Rev. D* **4**, 1261 (1971).
- [59] E. T. Boschitz, W. K. Roberts, J. S. Vincent, M. Blecher, K. Gotow, P. C. Gugelot, C. F. Perdrisat, L. W. Swenson, and J. R. Priest, Elastic Scattering of 600 MeV Protons from H, D, ${}^3\text{He}$, and ${}^4\text{He}$, *Phys. Rev. C* **6**, 457 (1972).
- [60] E. Winkelmann, P. R. Bevington, M. W. McNaughton, H. B. Willard, F. H. Cverna, E. P. Chamberlin, and N. S. P. King, Proton-deuteron elastic scattering at 800 MeV, *Phys. Rev. C* **21**, 2535 (1980).
- [61] K. Sagara, H. Oguri, S. Shimizu, K. Maeda, H. Nakamura, T. Nakashima, and S. Morinobu, Energy dependence of analyzing power A_y and cross section for $p + d$ scattering below 18 MeV, *Phys. Rev. C* **50**, 576 (1994).
- [62] K. Sekiguchi, H. Sakai, H. Witała, W. Glöckle, J. Golak, M. Hatano, H. Kamada, H. Kato, Y. Maeda, J. Nishikawa, A. Nogga, T. Ohnishi, H. Okamura, N. Sakamoto, S. Sakoda, Y. Satou, K. Suda, A. Tamii, T. Uesaka, T. Wakasa, and K. Yako, Complete set of precise deuteron analyzing powers at intermediate energies: Comparison with modern nuclear force predictions, *Phys. Rev. C* **65**, 034003 (2002).

- [63] K. Hatanaka, Y. Shimizu, D. Hirooka, J. Kamiya, Y. Kitamura, Y. Maeda, T. Noro, E. Obayashi, K. Sagara, T. Saito, H. Sakai, Y. Sakemi, K. Sekiguchi, A. Tamii, T. Wakasa, T. Yagita, K. Yako, H. P. Yoshida, V. P. Ladygin, H. Kamada, W. Glöckle, J. Golak, A. Nogga, and H. Witała, Cross section and complete set of proton spin observables in $\bar{p}d$ elastic scattering at 250 MeV, *Phys. Rev. C* **66**, 044002 (2002).
- [64] K. Ermisch, H. R. Amir-Ahmadi, A. M. van den Berg, R. Castelijn, B. Davids, A. Deltuva, E. Epelbaum, W. Glöckle, J. Golak, M. N. Harakeh, M. Hunyadi, M. A. de Huu, N. Kalantar-Nayestanaki, H. Kamada, M. Kiš, M. Mahjour-Shafiei, A. Nogga, P. U. Sauer, R. Skibiński, H. Witała, and H. J. Wörtche, Systematic investigation of three-nucleon force effects in elastic scattering of polarized protons from deuterons at intermediate energies, *Phys. Rev. C* **71**, 064004 (2005).
- [65] A. Koning and J. Delaroche, Local and global nucleon optical models from 1 keV to 200 MeV, *Nucl. Phys. A* **713**, 231 (2003).
- [66] H. An and C. Cai, Global deuteron optical model potential for the energy range up to 183 MeV, *Phys. Rev. C* **73**, 054605 (2006).
- [67] F. Perey and B. Buck, A non-local potential model for the scattering of neutrons by nuclei, *Nucl. Phys.* **32**, 353 (1962).
- [68] TWOFNR user manual.
- [69] S. Cohen and D. Kurath, Two-nucleon transfer in the $1p$ shell, *Nucl. Phys. A* **141**, 145 (1970).
- [70] J. Y. Grossiord, M. Bedjidian, A. Guichard, M. Gusakow, J. R. Pizzi, T. Delbar, G. Grégoire, and J. Lega, (p, pd) , (p, pt) and $(p, p^3\text{He})$ reactions on ^{12}C and ^{16}O at 75 MeV, *Phys. Rev. C* **15**, 843 (1977).
- [71] C. Kim, S. Bunch, D. Devins, and H. Forster, Elastic scattering of 31 MeV protons from H^2 , He^3 , N^{14} and O^{16} , *Nucl. Phys.* **58**, 32 (1964).
- [72] F. Hinterberger, G. Mairle, U. Schmidt-Rohr, G. Wagner, and P. Turek, Elastic scattering of 52 MeV deuterons, *Nucl. Phys. A* **111**, 265 (1968).
- [73] T. Y. Li and S. K. Mark, Optical model analysis of elastic scattering of 100-MeV protons from light nuclei, *Canadian Journal of Physics* **46**, 2645 (1968).
- [74] C. Rolland, B. Geoffrion, N. Marty, M. Morlet, B. Tatischeff, and A. Willis, Modele optique pour la diffusion elastique des protons de 75 MeV et 150 MeV, *Nuclear Physics* **80**, 625 (1966).
- [75] M. Gaillard, R. Bouché, L. Feuvrais, P. Gaillard, A. Guichard, M. Gusakow, J. Leonhardt, and J.-R. Pizzi, Comparaison des réactions $(d, ^3\text{He})$ ET (d, t) sur quelques noyaux $N = Z$, *Nuclear Physics A* **119**, 161 (1968).